water

MDPI

Article

Investigation of Hydraulic Performance Based on Response Surface Methodology for an Agricultural Chemigation Proportional Injector

Pan Tang, Chao Chen * and Hong Li

Research Centre of Fluid Machinery Engineering and Technology, Jiangsu University, Zhenjiang 212013, China; tangpan19@163.com (P.T.); hli@ujs.edu.cn (H.L.)

* Correspondence: chch3605@ujs.edu.cn; Tel.: +86-139-5140-1065

Received: 29 September 2020; Accepted: 9 November 2020; Published: 11 November 2020

Abstract: Injectors are key pieces of equipment for chemigation systems, and their hydraulic performance has a significant effect on chemigation systems and crops. In order to investigate the influence of different working parameters on hydraulic performance for a water-powered proportional injector (PI), three key parameters of inlet and injection flow rate were researched using a one-factor experimental design method. The regression equations between different factors and response variables were established through a response surface method based on one-factor experimental results. Lastly, a mathematical model of the actual injection ratio was established. Some experiments under different, randomly selected parameter combinations were carried out to verify the prediction precision of the mathematical mode. The results showed that the injection flow rate increased first within the differential pressure of 0.05 to 0.10 MPa and then tended towards stability with increasing differential pressure. The injection flow rate decreased by increasing the viscosity and the change in the injection flow rate was small enough when the viscosity was greater than 500 mPa·s. The impact factors, in order of significance, for inlet flow rate were differential pressure, viscosity of injection liquid and setting injection ratio. The impact factors, in order of significance, for injection flow rate were viscosity of injection liquid, setting injection ratio and differential pressure. The regressive model for predicting the actual injection ratio was validated using an experiment and the relative deviation between calculated value and tested value was less than 5.98%, which indicated that the mathematical model had high credibility.

Keywords: precision agriculture; chemigation; proportional injector; hydraulic performance; mathematical model; response surface methodology

1. Introduction

Chemigation is the injection of any chemical such as fertilizers, micronutrients, or pesticides into irrigation water and is applied to the land using an irrigation system. Fertigation is specifically the application of fertilizer through an irrigation system, and has been widely used throughout the world [1–3]. The proper use of chemigation is recognized as the best management practice for irrigated agriculture. Chemigation can effectively reduce labor and increase crop yield and quality; at the same time, the use of fertilizers and pesticides can be reduced, which is conducive to the sustainable development of the environment [4–6].

Injectors are key pieces of equipment for chemigation systems, and their hydraulic performance determines the quality of the chemigation system to a great extent [7–9]. At present, the commonly used injectors include the Venturi injector, differential pressure tanks, and other different types of pumps [10–12]. Many scholars have conducted detailed studies on Venturi injectors and differential pressure tanks [13–16]. A low equipment cost, low energy consumption and high injection precision

are necessary to improve the water and chemical distribution uniformity and realize the precise control of water and chemicals [17,18].

The operation of proportional injectors (PIs) relies on the pressure of the water flow without electricity, so that it can be used anywhere [6]. At present, PIs are widely used in fertigation systems for greenhouses and cash crops [19,20]. For this kind of injector, there were some studies that reported on its mechanical structure design. The Dosatron Company has led the development of a range of PIs designed to meet technical requirements specific to each area of operation [21]. Tang et al. [22] analyzed the force of the drive piston in the process of reciprocating motion, established a three-dimensional dynamic simulation model of a proportional pump through writing dynamic mesh programs according to a user defined function (UDF) and simulated the internal flow field of the proportional pump. Wang et al. [23] carried out a test to investigate the effect of fertilization proportion and fertilization–water ratio on the clogging of filters by fertilizer pumps in a micro-irrigation system. Li et al. [24] analyzed the structure principle and main performance parameters of a fertilization pump, and also carried out a hydraulic performance test, indicating that the injection ratio of the fertilization pump was relatively stable under different inlet and outlet pressure differences. Zhang et al. [25] designed an innovative piece of equipment with a simple structure to distribute solid fertilizer through a fertigation system. In actual engineering applications, Bracy [26], Tayel [27] and Li [11,15] successfully applied a PI as one kind of injector to inject fertilizer into irrigation water and indicated that the use of a PI can result in good water and fertilizer distribution uniformity because of the high injection precision of the Venturi injector. Fan et al. [8] also indicated that a fertigation system with PI achieved the highest fertilizer distribution uniformity.

For the development of the current application, the hydraulic performance of this type of injector in practical engineering applications should be studied further. Therefore, in this study, the inlet and injection flow rate were taken as indexes to analyze the influence of different working parameters based on the response surface method (RSM). Then the regression equations between differential pressure, setting injection ratio, the viscosity of injection liquid and the two indexes were established through the response surface method, respectively. Finally, the mathematical model was confirmed using an experiment.

2. Materials and Methods

2.1. Model Injector

Figure 1 shows the schematic diagram of the PI. It was installed directly into the water supply line and the injector operates without an electrical motor. It uses the flow of water as a power source activating the motor piston, which takes up the required percentage of concentrate and injects it into the water. Table 1 presents the technical parameters of the PI. The D25RE2 proportional injector from Dosatron International S.A.S (Tresses, France) was selected for this study. Table 1 presents the technical parameters of the PI.

Table 1. Technical parameters.

Inlet Diameter (mm)	Outlet Diameter (mm)	Working Pressure (MPa)	Setting Injection Ratio (%)
19	19	0.02~0.6	0.2~2.0

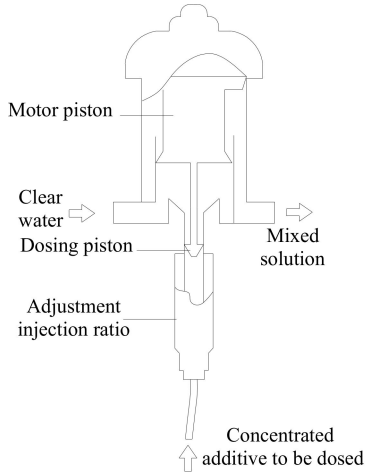

Figure 1. Schematic diagram of proportional injector (PI).

2.2. Experimental Setup

Figure 2 presents a structural diagram of the test system. A centrifugal pump with a flow rate of 10 m^3 h^{-1} and a lift head of 70 m delivered water to the system. The flow rate was measured by an electromagnetic flowmeter with an accuracy of ±0.3%. The injection flow rate of the PI was measured by an electronic balance with an accuracy of 0.1 g. Three pressure gauges with an accuracy of ±0.4% were installed to monitor the differential pressure.

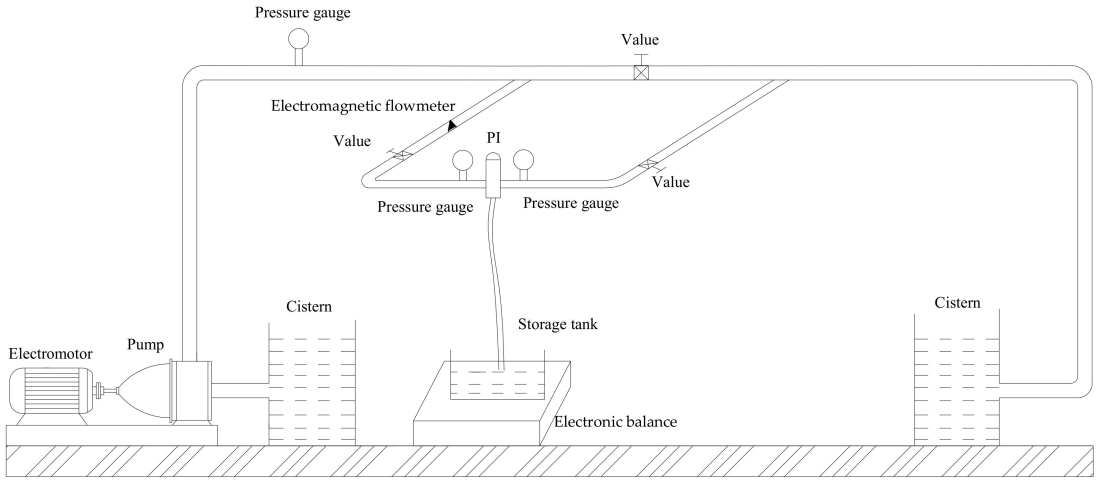

Figure 2. Structural diagram of experimental setup.

2.3. Preparation of Different Viscosity Solution

Since water and glycerin can be dissolved in any ratio and the viscosity of water at 20 degrees is 1 mPa·s, solutions with different viscosities can be obtained by controlling the ratio of glycerin to water. The viscosity values for each test were measured using an NDJ-5S rotary viscosity meter (Shanghai lichen bangxi instrument technology Co. Ltd., Shanghai, China) with an accuracy of ±2%.

2.4. One-Factor Experimental Design Method

During the experiment, the optimal parameter ranges of the response surface method were firstly determined by a one-factor experimental design method.

Differential pressure: Inlet flow rate (Q_{il}) and injection flow rate (Q_{ij}) were tested with different differential pressures of 0.05, 0.10, 0.15, 0.20, 0.25, 0.30, 0.35 and 0.40 MPa when the setting injection ratio was 1.0% and the viscosity of injection liquid was 1 mPa·s.

Setting injection ratio: Q_{il} and Q_{ij} were tested with different setting injection ratios of 0.2%, 0.3%, 0.4%, 0.5%, 0.6%, 0.7%, 0.8%, 1.0%, 1.2%, 1.4%, 1.6%, 1.8% and 2.0% when the differential pressure was 0.10 MPa and the viscosity of injection liquid was 1 mPa·s.

Viscosity of injection liquid: Q_{il} and Q_{ij} were tested with injection liquids with different viscosities of 1, 50, 150, 200, 250, 300, 350, 400, 450, 500, 550 and 600 mPa·s when the differential pressure was 0.10 MPa and the setting injection ratio was 1.0%.

The inlet flow rate was obtained directly from the electromagnetic flowmeter. The injection flow rate was obtained by the following equation:

$$Q = \frac{m_1 - m_2}{t} \quad (1)$$

where Q is the injection flow rate (kg h^{-1}), m_1 is the initial mass of the storage tank with injected liquid (kg), m_2 is the final mass of the storage tank with injected liquid (kg), and t is the measurement time (h)—the time was 0.5 h in this research. The averages of three repeated experimental results were adopted as the final results.

2.5. Response Surface Method

Based on the one-factor experimental results, the three factors that affected inlet flow rate and injection flow rate were investigated by the response surface method (RSM). RSM is a collection of mathematical and statistical techniques for researching problems in which several independent factors have effect on response variables, which contain the main methods of Box–Behnken and central composite design [28,29]. RSM aims at building a regression model (approximation) that is closest to the true regression model. The model to be built is based on experimental data and the model is empirical [30]. This mathematical regression model can be used to predict the response values. Hence, the RSM was adopted in this study.

In order to ensure the accuracy of the experiment and reduce the experimental schemes, Box–Behnken design (BBD) was chosen in this study. BBD is considered to be more proficient and most powerful than other designs such as three-level full factorial design, central composite design and Doehlert design. Box–Behnken designs are used to generate higher order response surfaces using fewer required runs than a normal factorial technique. Figure 3 presents the BBD model, and the central points of space and edges were the experimental design points.

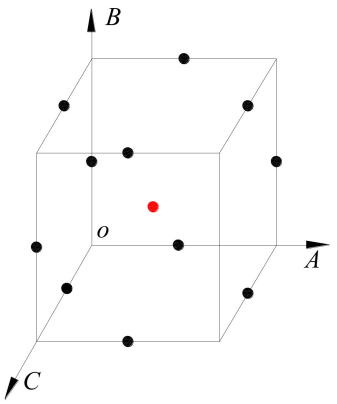

Figure 3. Box–Behnken design model for three levels.

2.6. Statistical Analyses

The *p*-test is a statistical method that tests the validity of the null hypothesis which states a commonly accepted claim about a population [31]. The smaller the *p*-value, the stronger the evidence that the null hypothesis should be rejected and that the alternate hypothesis might be more credible. Researchers will usually choose alpha levels of 5% or lower, which translate to confidence levels of 95% or greater. In other words, a *p*-value less than a 5% alpha level means that there is a greater than 95% chance that your results are not random, thus enhancing the significance of your results. The *p*-value has its fixed calculation method. The Design-Expert software was used in this study for data processing, and the *p*-value can be obtained directly from the software.

3. Results and Discussion

3.1. Analysis of One-Factor Experimental Results

Figure 4 presents the influence of differential pressure on Q_{il} and Q_{ij}, respectively. It can be seen that the Q_{ij} increased first and then remained at a certain level with increasing differential pressure, which indicated that it was useless to increase the Q_{il} by merely increasing differential pressure. The best working condition appeared when differential pressure was 0.10 MPa. The Q_{il} increased with increasing differential pressure, and basically showing linear change. Hence, the selected differential pressure range for RSM was determined from 0.05 to 0.15 MPa. Han et al. [32] analyzed the injection performance of three types of proportional injectors through experimental research, and pointed out that the injection flow rate of the proportional injectors was affected by the differential pressure, the operating conditions of high pressure and large flow will affect the injection performance, the inlet flow rate should not exceed the design flow rate when the proportional injector is working, and the inlet flow rate should not be too large when the injection ratio is small.

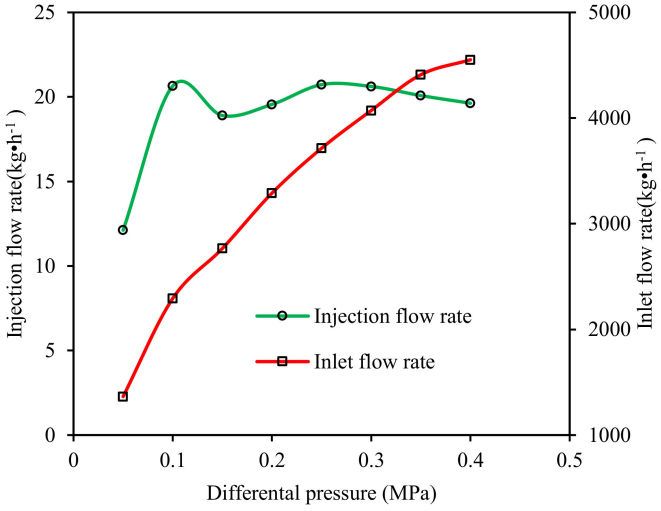

Figure 4. Influence of differential pressures on Q_{il} and Q_{ij}.

Figure 5 presents the influence of setting the injection ratio on Q_{il} and Q_{ij}, respectively. It was shown that the Q_{ij} increased and the Q_{il} decreased with an increasing setting injection ratio, and the relationships between Q_{ij}, Q_{il} and the setting injection ratio remained approximately linear. Moreover, the selected setting injection ratio range for RSM was determined from 0.2% to 2.0%, which means the full range of the PI. Wu et al. [33] conducted an experiment on a proportional injector and indicated that, under the same injection ratio, the outlet of the mass percentage concentration of the fertilizer solution after entering the main pipe essentially did not change with time and it was recommended that, in order to improve the accuracy of injected fertilizer, the proportional injector should not use a large pressure difference and a small injection ratio during operation.

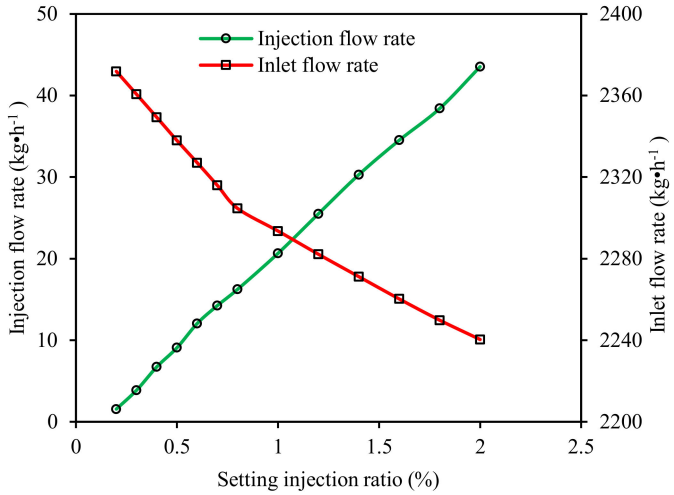

Figure 5. Influence of setting injection rate on Q_{il} and Q_{ij}.

Figure 6 presents the influence of the viscosity of the injection liquid on Q_{il} and Q_{ij}, respectively. It can be seen that Q_{il} increased and Q_{ij} decreased with the increasing viscosity of the injection liquid. Tang et al. [9] also indicated that when the injected liquid viscosity was less than 20 mPa·s, the viscosity had little effect on the Q_{ij}. The Q_{ij} was tending towards stability when the viscosity of the injection liquid was greater than 500 mPa·s. Furthermore, two curves in Figure 6 were comparatively analyzed and the results showed that the growth rate of Q_{il} when the viscosity of the injection liquid was less than 500 mPa·s was significantly lower than the growth rate of Q_{il} when the viscosity of the injection liquid exceeded 500 mPa·s. Hence, the selected viscosity of the injection liquid range for RSM was determined from 1 to 500 mPa·s according to the results. When the viscosity of the sucked liquid increases, the resistance of the suction piston will increase, and more energy is needed to drive the piston to reciprocate. This is the reason why Q_{il} increased with increasing viscosity.

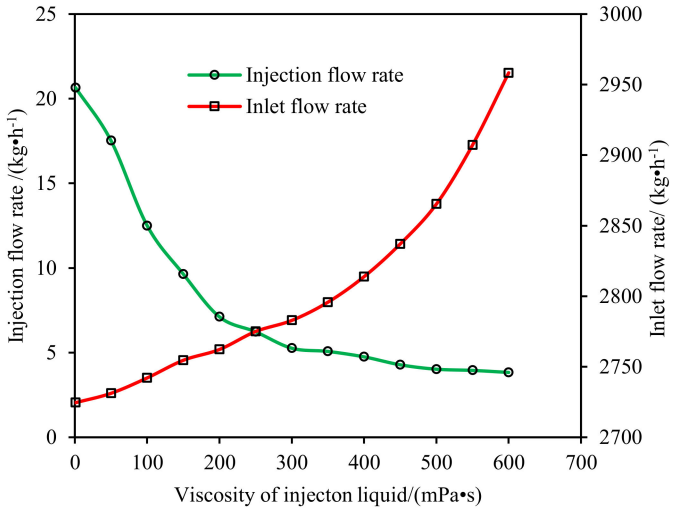

Figure 6. Influence of viscosity of injection liquid on Q_{il} and Q_{ij}.

3.2. Model Fitness and Adequacy Verification

Therefore, three factors and three levels of experiment need to be designed. Table 2 presents the test table of three levels and three factors based on BBD [34].

Table 2. Experimental factor and levels.

Code	Factor		
	Differential Pressure *A* (MPa)	**Setting Injection Ratio *B* (%)**	**Viscosity of Injection Liquid *C* (MPa·s)**
1	0.15	2.0	500.0
0	0.10	1.1	250.5
−1	0.05	0.2	1.0

According to the BBD method, 17 group schemes in Table 3 were determined and the response variables of each scheme were tested by an experiment. The Design-Expert software (Stat-Ease, Inc. Minneapolis, MN, USA) was applied to the RSM to obtain the relationship between different factors and objective functions. More importantly, the mathematical models were built by using regression analysis.

Table 3. Response surface experimental design and results.

No.	*A* (MPa)	*B* (%)	*C* (mPa·s)	Q_{il} (kg·h^{-1})	Q_{ij} (kg·h^{-1})
1	0.15	0.20	250.5	2664.11	1.22
2	0.10	1.10	250.5	2190.94	5.48
3	0.15	1.10	1.0	2739.45	24.36
4	0.05	1.10	1.0	1358.02	17.52
5	0.10	1.10	250.5	2187.33	6.61
6	0.05	0.20	250.5	1289.41	1.05
7	0.05	2.00	250.5	1095.31	9.43
8	0.10	1.10	250.5	2176.26	4.15
9	0.15	1.10	500.0	2802.67	1.40
10	0.05	1.10	500.0	1195.06	3.01
11	0.10	0.20	1.0	2318.52	2.56
12	0.10	1.10	250.5	2159.09	4.13
13	0.10	2.00	1.0	2240.36	39.53
14	0.15	2.00	250.5	2797.12	18.55
15	0.10	0.20	500.0	2240.07	1.82
16	0.10	2.00	500.0	2167.83	1.81
17	0.10	1.10	250.5	2170.38	5.13

The quadratic polynomial equations for the response variables using relative parameters were established as described below in Equations (2) and (3):

$$Q_{il} = 239.08 + 29357.74A - 216.26B - 1.1C + 1817.28AB + 4.53AC + 0.0066BC - 86641.5A^2 + 1.59B^2 + 0.001C^2 \quad (2)$$

$$Q_{ij} = 3.46 - 80.18A + 10.89B - 0.02C + 49.72AB - 0.17AC - 0.04BC + 521A^2 + 1.43B^2 + 0.00008C^2 \quad (3)$$

where *A* is differential pressure, MPa; *B* is the setting injection ratio, %; *C* is the viscosity of the injection liquid, mPa·s.

The adequacy of the mathematical models was tested by using the analysis of variance technique and the results of the second order response surface model fitting in the form of an analysis of variance. The analyses of variance for Q_{il} and Q_{ij} are shown in Tables 4 and 5, respectively. If the calculated *F*-value of the mathematical model is less than the standard *F*-value, which, according to the *F* table, can be found using a desired level of confidence of 95%, then the mathematical model is said to be adequate and within the confidence level [35]. From Tables 4 and 5, the generated quadratic models were observed to be significant and they were proved by the model *F*-value (1282.71 and 61.13). The *p*-values for the two mathematical models were less than 0.05, which indicated that the models were significant and the lack of fit was significant.

Table 4. Analysis of variance table for the Q_{il}.

Source	Sum of Squares	Df	Mean Square	*F*-Value	*p*-Value	Significant
Model	4,861,000	9	540,100	1282.71	<0.0001	***
A	4,599,000	1	4,599,000	10,921.53	<0.0001	***
B	5591.00	1	5591.00	13.28	0.0082	**
C	7857.56	1	7857.56	18.66	0.0035	**
AB	26,750.24	1	26,750.24	63.53	<0.0001	***
AC	12,789.35	1	12,789.35	30.37	0.0009	**
BC	8.76	1	8.76	0.021	0.8894	
A^2	197,500	1	197,500	469.14	<0.0001	***
B^2	7.02	1	7.02	0.017	0.9009	
C^2	17,033.42	1	17,033.42	40.45	0.0004	***
Residual	2947.57	7	421.08			
Lack of Fit	2281.60	3	760.53	4.57	0.0882	
Pure Error	665.97	4	166.49			
Total	4,864,000	16				

Note: ** means $p < 0.01$, *** means $p < 0.001$.

Table 5. Analysis of variance table for the Q_{ij}.

Source	Sum of Squares	Df	Mean Square	*F*-Value	*p*-Value	Significant
Model	1750.51	9	194.50	61.13	<0.0001	***
A	26.35	1	26.35	8.28	0.0237	*
B	490.94	1	490.94	154.30	<0.0001	***
C	720.67	1	720.67	226.50	<0.0001	***
AB	20.03	1	20.03	6.29	0.0405	*
AC	17.85	1	17.85	5.61	0.0497	*
BC	341.88	1	341.88	107.45	<0.0001	***
A^2	7.14	1	7.14	2.25	0.1777	
B^2	5.67	1	5.67	1.78	0.2238	
C^2	112.54	1	112.54	35.37	0.0006	***
Residual	22.27	7	3.18			
Lack of Fit	18.00	3	6.00	5.62	0.0643	
Pure Error	4.27	4	1.07			
Total	1772.79	16				

Note: * means $p < 0.05$, *** means $p < 0.001$.

The degree of different factors on response variables can be obtained from the *F*-value from Tables 4 and 5. According to the *F*-value in Table 4, the Q_{il} was mostly affected by *A*, *C* and *B*. According to the *F*-value in Table 5, the Q_{ij} was mostly affected by *C*, *B* and *A*.

An analysis of variance was used to investigate the statistical significance of the regression coefficients. For each of the terms in the models, the larger the magnitude of the *F*-values and the smaller the *p*-values, the more significant the corresponding coefficients were. For Equation (2), the relative analysis of variance (Table 4) showed that the Q_{il} significantly depended on the three selected individual dependent variables *A*, *B*, *C* and quadratic model factors A^2, C^2 and the two interactive model terms *AB*, *AC*. For Equation (3), the relative analysis of variance (Table 5) showed that the Q_{ij} significantly depended on the three selected individual dependent variables *A*, *B*, *C*, the quadratic model factors A^2, B^2 and C^2 and the two interactive model terms *AB*, *AC*, *BC*.

Table 6 presents the results of the regression analysis for Equations (2) and (3). The R-Squared and Adequate Precision values were worked out using the Design-Expert software. The R-Squared values for the models were observed to be 0.9994 and 0.9874, indicating a better fit between the mathematical models and the actual data observed within the experimental domain. For Equation (2), the predicted R-Squared value of 0.9923 was in reasonable agreement with the adjusted R-Squared of

0.9986. For Equation (3), the predicted R-Squared value of 0.8338 was also in reasonable agreement with the adjusted R-Squared value of 0.9713. Adequate Precision measures the signal-to-noise ratio and a ratio greater than four is desirable. The values of Adequate Precision for Equations (2) and (3) were considerably larger than four, and proved the required model discrimination. All the above considerations indicate the excellent adequacy of the regression models.

Table 6. Regression analysis for mathematical model.

Mathematical Model	R-Squared	Adj R-Squared	Pred. R-Squared	Adeq. Precision
Equation (2)	0.9994	0.9986	0.9923	108.786
Equation (3)	0.9874	0.9713	0.8338	28.284

Note: R-Squared is coefficient of determination; Pred. R-Squared is predicted R-Squared; Adj R-Squared is adjusted R-Squared; Adeq. Precision is Adequate Precision.

After determining the significant coefficients, the final regressive model was built to predict the inlet flow rate (Equation (4)) and injection flow rate (Equation (5)) of the PI, as given below:

$$Q_{il} = 239.08 + 29357.74A - 216.26B - 1.1C + 1817.28AB + 4.53AC - 86641.5A^2 + 0.001C^2 \quad (4)$$

$$Q_{ij} = 3.46 - 80.18A + 10.89B - 0.02C + 49.72AB - 0.17AC - 0.04BC + 0.00008C^2 \quad (5)$$

Figure 7 presents the normal percentage probability versus residual plots for Q_{il} and Q_{ij}. It can be seen that the residual points are distributed almost in a straight line, which indicates that the mathematical model established in this article fitted well.

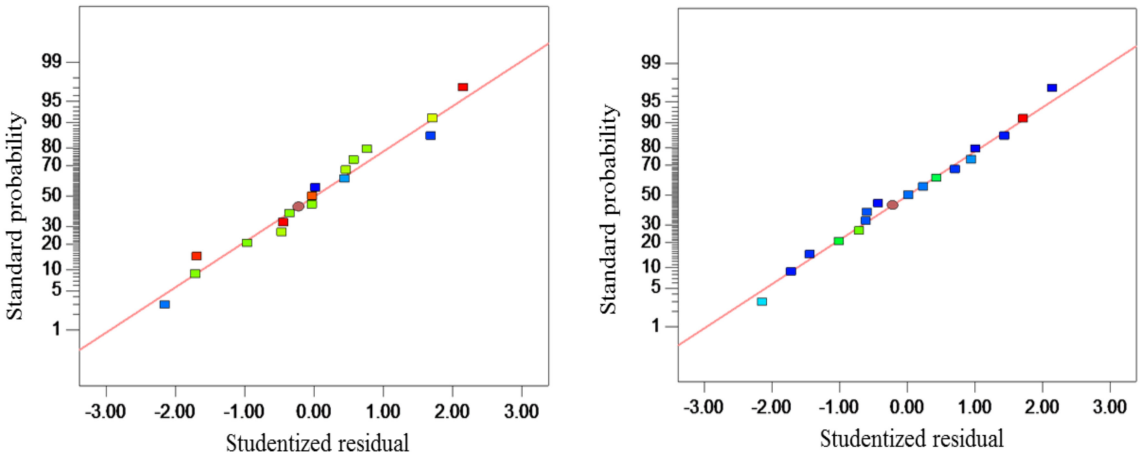

Figure 7. Normal plots of residuals for the responses. (**a**) Q_{il}; (**b**) Q_{ij}.

Figure 8 presents the predicted value versus the tested value of the response variable from the mathematical models. The data points of the two responses were relatively close to the 45° line, which revealed that there was a very good correlation between the tested value and predicted value [36]. Moreover, the good distribution of data in Figure 8a,b indicated that the choice of the selected parameters and their levels were acceptable.

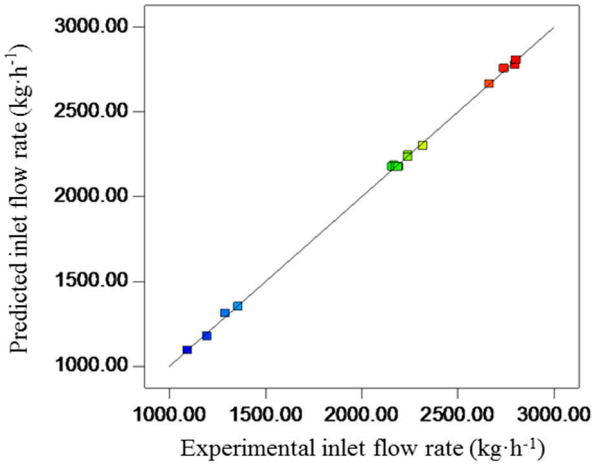

(**a**)

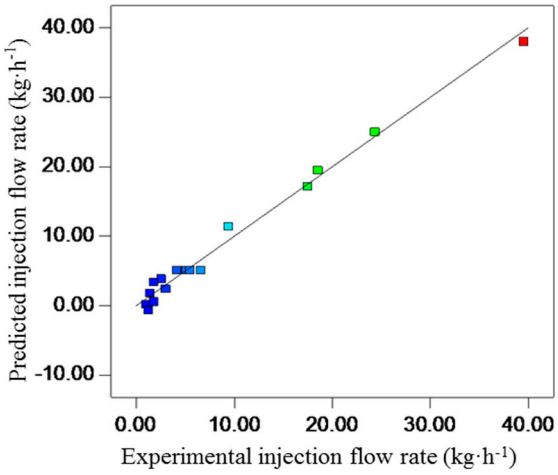

(**b**)

Figure 8. Plot of actual values versus predicted values: (**a**) Q_{il}; (**b**) Q_{ij}.

3.3. Response Surface Analysis

One of the best methods to understand the effects of independent variables on the response are to utilize two-dimensional contour graphs of the model. Such equations were used to generate two-dimensional contour graphs by fixing one independent variable at the zero level while the others are varied within the range of study to further analyze the effects of independent variables on the responses. The main effects and interactive effects of the independent factors can be visually found in the contour graphs, and this also gives a visual representation of the values of the response.

Figure 9 presents the contour of interaction influence between different factors and Q_{il}, as can be seen in Figure 9a, which displays the contour graphs of the interaction between *A* and *B* on Q_{il} with *C* of 250.5 mPa·s. This indicated that the Q_{il} decreased with increasing *B*, and Q_{il} changed slightly when *A* increased to a threshold level (0.10 MPa). The effects of *A* and *C* on Q_{il} with a *B* of 1.1% are shown in Figure 9b. It can be seen from Figure 9b that the Q_{il} was mainly affected by *A*. *C* had a significant effect on Q_{il} with a lower *A*.

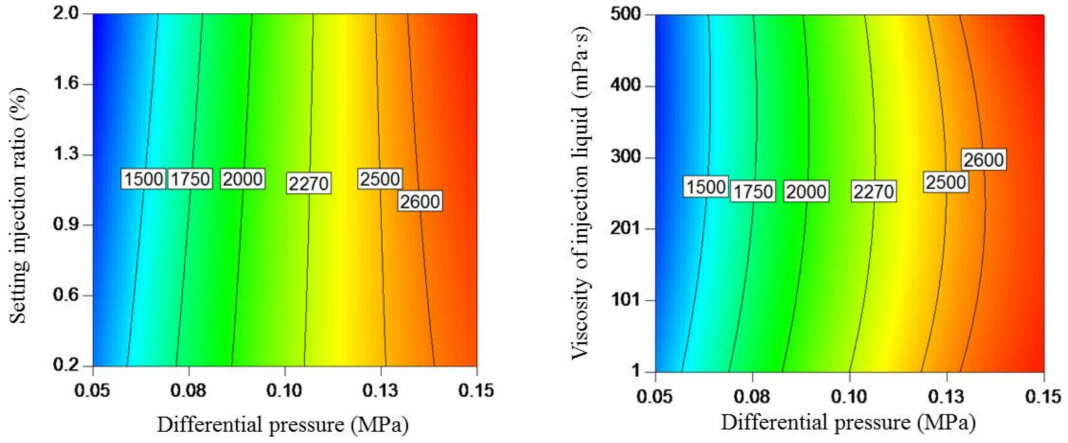

Figure 9. Contour of interaction influence between different factors and Q_{il}: (**a**) effect of *A* and *B*; (**b**) effect of *A* and *C*.

Figure 10a presents the contour graphs of the interaction influence between *A* and *B* on Q_{ij} with a *C* of 250.5 mPa·s. When *B* was lower than 1.0%, the Q_{ij} increased first and then decreased with the increase in *A*. When *B* was greater than 1.0%, the Q_{ij} was significantly decreased with increasing *A*. It thus can be concluded that the lower *A* should be adopted when *B* is greater than 1.0% in actual engineering applications.

Figure 10b presents the effects of *A* and *C* on Q_{ij} with a *B* of 1.1%. It was reported that the contour plots was stable with an *A* lower than 0.10 MPa and a *C* greater than 250 mPa·s, which indicated that the *A* had less of an impact on Q_{ij} under the above working conditions.

Figure 10c presents the effects of *B* and *C* on Q_{ij} with an *A* of 0.10 MPa. The shape of the contour illustrated the high *B* and low *C* and the response value also changed rapidly with increasing *B* and decreasing *C*. Meanwhile, it can be concluded that the interaction effect of *B* and *C* was higher than other interaction effects.

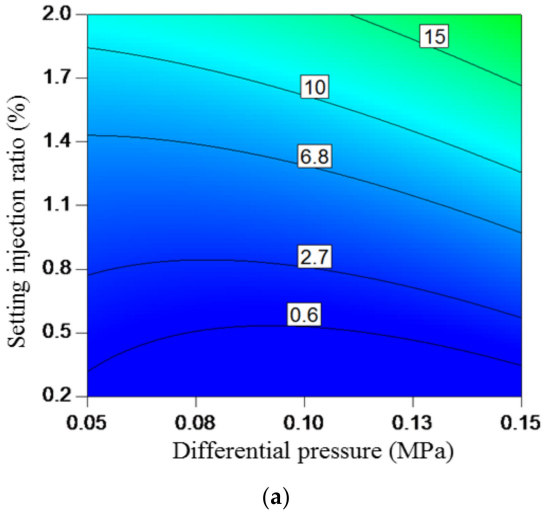

Figure 10. Cont.

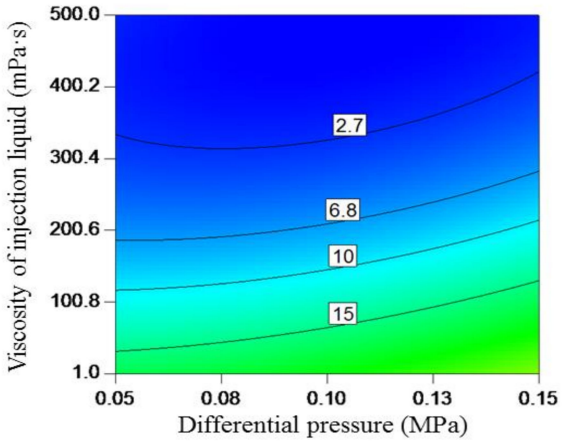

(**b**)

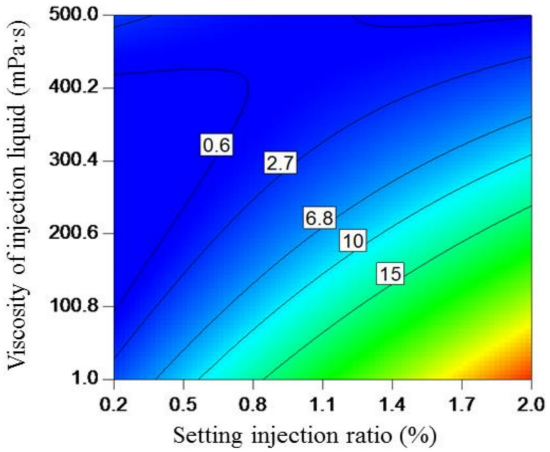

(**c**)

Figure 10. Contour of interaction influence between different factors and Q_{ij}: (**a**) effect of *A* and *B*; (**b**) effect of *A* and *C*, (**c**) effect of *B* and *C*.

4. Confirmation Experiment

Six group schemes with different factor combinations were carried out to validate the mathematical models. Those six group schemes were selected by the no-repeat randomly selected function of Excel. An injection ratio with different *A*, *B* and *C* values can be calculated as:

$$r_{act} = \frac{Q_{ij}}{Q_{il}} \times 100 \quad (6)$$

where r_{act} is the actual injection ratio (%).

Table 7 presents the parameters of six group schemes and the comparison analysis results for the mathematical models. As can be seen in Table 7, the maximum relative error for the actual injection ratio between the calculated value and experimental value was −5.98%. The good agreement between the calculated value and experimental value verified the validity of the mathematical models, and indicated that the mathematical models can be used for predictions. Tang et al. [9] also established two mathematical calculation models for calculating Q_{il} and Q_{ij} for a proportional injector, and the determination coefficients of the two models were 0.8316 and 0.9706. However, the viscosity of the injected liquid was only up to 250 mPa·s, and the application range was not wide.

Table 7. Test results under different random combinations.

Characteristic	Values					
A (MPa)	0.13	0.06	0.12	0.07	0.15	0.09
B (%)	1.0	0.3	0.9	0.4	1.2	0.6
C (mPa·s)	98	449	328	115	185	242
Calculated value of Q_{il} (kg h^{-1})	2570.85	1486.21	2441.09	1757.15	2717.34	2038.88
Calculated value of Q_{ij} (kg h^{-1})	13.21	1.86	1.20	1.87	11.98	0.53
Calculated value of injection ratio (%)	0.51	0.13	0.05	0.11	0.44	0.03
Tested value of Q_{il} (kg h^{-1})	2657.15	1564.34	2341.28	1878.37	2579.66	2134.03
Tested value of Q_{ij} (kg h^{-1})	14.36	2.15	1.22	2.2	11.84	0.62
Tested value of injection ratio (%)	0.54	0.137	0.052	0.117	0.459	0.029
Relative error for injection ratio (%)	−5.56	−5.11	−3.85	−5.98	4.14	3.45

5. Conclusions

This article presents the differential pressure, setting injection ratio and viscosity of injection liquid on the hydraulic performance of PI. From the results of this study, the following conclusions can be drawn:

For the one-factor experimental design method condition, the inlet flow rate increased with increasing differential pressure and the viscosity of the injection liquid and decreased with an increasing setting injection ratio. The injection flow rate increased with increasing differential pressure within a differential pressure of 0.05 to 0.10 MPa and decreased with the increasing viscosity of the injection liquid.

The impact factors, in order of significance, for inlet flow rate were differential pressure, viscosity of injection liquid and setting injection ratio. The impact factors, in order of significance, for injection flow rate were viscosity of injection liquid, setting injection ratio and differential pressure. All of the three selected factors had a significant influence on the inlet flow rate and injection flow rate. The mathematical model can be used to predict the actual injection ratio within the relative error between predicted values and the experimental values were less than 5.98%.

The information provided in this article can contribute to actual engineering applications. Further research should focus on the internal flowing mechanism of PIs, which will help to optimize the design of hydraulic parts. At the same time, only one D25RE2 proportional injector (as a model injector) was tested to establish the prediction models in this study. In future research, on the one hand, we will use more proportional injectors of the same series to verify the prediction model. On the other hand, we will also investigate different series of products (different inlet and outlet diameters, different working pressures, etc.) to build a universal mathematical model that can finally be applied to all products.

Author Contributions: P.T. conceived and structured the testing system. H.L. performed the literature search, helped with the experiments and analyzed the test data. P.T. and C.C. wrote the paper and approved the submitted version of the manuscript. All authors have read and agreed to the published version of the manuscript.

Funding: This work was supported by the National Natural Science Foundation of China (51939005), Natural Science Research Project of Jiangsu Higher Education Institutions (19KJB470014), Jiangsu Agriculture Science and Technology Innovation Fund (CX(19)2040), and a project funded by the Priority Academic Program Development of Jiangsu Higher Education Institutions (No. PAPD-2018-87).

Acknowledgments: Special thanks are due to the editor and reviewers for their valuable comments that helped improve the quality of this paper.

Conflicts of Interest: The authors declare no conflict of interest.

References

1. Tang, P.; Li, H.; Issaka, Z.; Chen, C. Effect of manifold layout and fertilizer solution concentration on fertilization and flushing times and uniformity of drip irrigation systems. *Agric. Water Manag.* **2018**, *200*, 71–79. [CrossRef]
2. Tu, Q.; Yi, M.; L, H.; Zhang, K.; Zhang, Q.K. Effect of solution concentration on fertigation uniformity of impact sprinkler. *J. Drain. Irrig. Mach. Eng.* **2020**, *38*, 1180–1188.
3. Rasool, G.; Guo, X.P.; Wang, Z.C.; Ali, M.U.; Chen, S.; Zhang, S.X.; Wu, Q.J.; Ullah, M.S. Coupling fertigation and buried straw layer improves fertilizer use efficiency, fruit yield, and quality of greenhouse tomato. *Agric. Water Manag.* **2020**, *239*, 106239. [CrossRef]
4. Li, Y.B.; Liu, J.P. Prospects for development of water saving irrigation equipment and technology in China. *J. Drain. Irrig. Mach. Eng.* **2020**, *38*, 738–742.
5. Leib, B.G.; Jarrett, A.R.; Orzolek, M.D.; Mumma, R.O. Drip chemigation of imidacloprid under plastic mulch increased yield and decreased leaching caused by rainfall. *Trans. ASAE* **2000**, *43*, 615. [CrossRef]
6. Zou, L.Y.; Chen, Z.; Duan, F.Y.; Ma, C.Y.; Fan, Y.S. Effects of water-fertilizer interaltion with planting density on water and nitrogen use efficiency and yield of winter wheat under sprinkler irrigation system. *J. Drain. Irrig. Mach. Eng.* **2020**, *38*, 632–636.
7. Manzano, J.; Palau, C.V.; Azevedo, B.M.D.; Bomfim, G.V.D.; Vasconcelos, D.V. Characterization and selection method of Venturi injectors for pressurized irrigation. *Rev. Ciênc. Agronôm.* **2018**, *49*, 201–210. [CrossRef]
8. Fan, J.L.; Wu, L.; Zhang, F.C.; Yan, S.; Xiang, Y. Evaluation of drip fertigation uniformity affected by injector type, pressure difference and lateral layout. *Irrig. Drain.* **2017**, *66*, 520–529. [CrossRef]
9. Tang, P.; Li, H.; Issaka, Z.; Chen, C. Methodology to investigate the hydraulic characteristics of a water-powered piston-type proportional injector used for agricultural chemigation. *Appl. Eng. Agric.* **2018**, *34*, 545–553. [CrossRef]
10. Wang, Q.L.; Wang, Z.H.; Wu, W.Y.; Liao, R.K. Throat structure optimization and flow field analysis of ATP Venturi fertilizer applicators. *J. Drain. Irrig. Mach. Eng.* **2018**, *36*, 829–834.
11. Li, J.S.; Du, Z.; Li, Y. Field evaluation of fertigation uniformity for subsurface drip irrigation systems. *Trans. Chin. Soc. Agric. Eng.* **2008**, *24*, 83–87.
12. Wang, H.T.; Chen, Y.Y.; Wang, J.D.; Yang, B.; Mo, Y. Experimental study on comprehensive working performance of Venturi injector. *J. Drain. Irrig. Mach. Eng.* **2018**, *36*, 340–346.
13. Manzano, J.; Palau, C.V.; Benito, M.; Guilherme, V.; Vasconcelos, D.V. Geometry and head loss in Venturi injectors through computational fluid dynamics. *Eng. Agríc.* **2016**, *36*, 482–491. [CrossRef]
14. Wang, H.T.; Wang, J.D.; Yang, B.; Mo, Y. Numerical simulation of Venturi injector with non-axis-symmetric structure. *J. Drain. Irrig. Mach. Eng.* **2018**, *36*, 1098–1103.
15. Li, J.S.; Meng, Y.B.; Li, B. Field evaluation of fertigation uniformity as affected by injector type and manufacturing variability of emitters. *Irrig. Sci.* **2007**, *25*, 117–125. [CrossRef]
16. Li, J.S.; Meng, Y.B.; Liu, Y.C. Hydraulic performance of differential pressure tanks for fertigation. *Trans. ASABE* **2006**, *49*, 1815–1822. [CrossRef]
17. Coates, R.W.; Sahoo, P.K.; Schwankl, L.J.; Delwiche, M.J. Fertigation techniques for use with multiple hydrozones in simultaneous operation. *Precis. Agric.* **2012**, *13*, 219–235. [CrossRef]
18. Wang, H.T.; Wang, J.D.; Yang, B.; Guo, S.Q.; Mo, Y.; Zhang, Y.Q. Effect of pipeline layout of fertilizer applicator on performance of Venturi injector. *J. Drain. Irrig. Mach. Eng.* **2019**, *37*, 534–539.
19. Janat, M. Efficiency of nitrogen fertilizer for potato under fertigation utilizing a nitrogen tracer technique. *Commun. Soil Sci. Plant Anal.* **2007**, *38*, 2401–2422. [CrossRef]
20. Kumar, M.; Kumar, R. Hydraulics of water and nutrient application through drip irrigation—A review. *J. Soil Water Conserv.* **2018**, *17*, 65–74. [CrossRef]
21. Dosatron Company [EB/OL]. (2017). Available online: http://www.dosatron.com/content/water-powered-dosing-technology (accessed on 7 June 2020).
22. Tang, P.; Li, H.; Luo, Z.W.; Sun, C.Z. Force analysis of drive piston and simulation and experiment of internal flow for proportional fertilizer pump. *Trans. Chin. Soc. Agric. Eng.* **2017**, *33*, 93–100.
23. Wang, R.; Wang, W.E.; Hu, X.T.; Yang, X.; Li, H.X. Impact of fertilizer proportion and fertilizer-water ratio on clogging of filter by fertilizer pump in microirrigation. *Trans. Chin. Soc. Agric. Eng.* **2017**, *33*, 117–122.

24. Li, H.; Zhang, Q.K.; Tang, P.; Sun, C.Z. Performance analysis and test of valve-regulated proportional fertilization pumps. *Trans. Chin. Soc. Agric. Eng.* **2020**, *36*, 34–41.
25. Zhang, Z.; Chen, C.; Li, H.; Xia, H. Design, development, and performance evaluation of a fertigation device for distributing solid fertilizer. *Water* **2020**, *12*, 2621. [CrossRef]
26. Bracy, R.P.; Parish, R.L.; Rosendale, R.M. Fertigation uniformity affected by injector type. *Horttechnology* **2003**, *13*, 103–105. [CrossRef]
27. Tayel, M.Y.; Eldardiry, E.I.; Shaaban, S.M.; Sabreen, K.P. Effect of injector types and irrigation and nitrogen levels on, III-cost analysis of garlic production. *J. Appl. Sci. Res.* **2010**, *6*, 822–829.
28. Ayim, I.; Ma, H.L.; Alenyorege, E.A. Optimizing and predicting degree of hydrolysis of ultrasound assisted sodium hydroxide extraction of protein from tea (*Camellia sinensis* L.) residue using response surface methodology. *J. Food Sci. Technol.* **2018**, *55*, 5166–5174. [CrossRef]
29. Dadzie, R.G.; Ma, H.L.; Abano, E.E.; Qu, W.J.; Mao, S.Y. Optimization of process conditions for production of angiotensin I-converting enzyme (ACE) inhibitory peptides from vital wheat gluten using response surface methodology. *Food Sci. Biotechnol.* **2013**, *22*, 1531–1537. [CrossRef]
30. Li, J.H.; Han, Y.Y.; Mao, G.P.; Wang, P. Optimization of exhaust emissions from marine engine fueled with LNG/diesel using response surface methodology. *Energy Sourcespart A* **2020**, *42*, 1436–1448. [CrossRef]
31. Francik, R.; Kryczyk-Kozioł, J.; Francik, S.; Gryboś, R.; Krośniak, M. Bis (4, 4′-dimethyl-2, 2′-bipyridine) oxidovanadium (IV) sulfate dehydrate: Potential candidate for controlling lipid metabolism? *Biomed. Res. Int.* **2017**, *2017*, 6950516. [CrossRef]
32. Han, Q.B.; Wu, W.Y.; Liu, H.L.; Huang, X.F.; Hao, Z.Y. Experiment on fertilizer injection performance of three hydraulic driven pumps. *Trans. Chin. Soc. Agric. Eng.* **2010**, *26*, 43–47.
33. Wu, X.K.; Wang, W.E.; Hu, X.T.; Wang, R.; Wu, W.Y. Experimental research on the influencing factors of performance of hydraulic driven proportional fertilizer. *China Rural Water Hydropower* **2018**, *4*, 6–9.
34. Zhang, L.; Gao, W.G.; Zhang, D.; Chang, W.F.; Nie, Y.X. Rapid evaluation of machine tools with position-dependent milling stability based on response surface model. *Adv. Mech. Eng.* **2016**, *8*, 1–12.
35. Adalarasan, R.; Santhanakumar, M.; Rajmohan, M. Optimization of laser cutting parameters for Al6061/SiCp/Al_2O_3, composite using grey based response surface methodology (GRSM). *Measurement* **2015**, *73*, 596–606.
36. Kadaganchi, R.; Gankidi, M.R.; Gokhale, H. Optimization of process parameters of aluminum alloy AA 2014-T6 friction stir welds by response surface methodology. *Def. Technol.* **2015**, *11*, 251–252.